Geochemical Perspectives Letters

Molybdenum isotope constraints on the temporal development of sulfidic conditions during Mediterranean sapropel intervals

T.C. Sweere, R. Hennekam, D. Vance, G-J. Reichart

Supplementary Information

The Supplementary Information includes:

- Material and Methods
- Results
- Comparison with Other Sapropel S5 Data
- Alternative Models for Low δ^{98}Mo Values
- Supplementary Information References

Material and Methods

The multi-core (MC, containing sapropel S1) and piston core (PC, containing sapropels S3 to S9) at location 64PE406-E1 (33°18.1'N, 33°23.7'E) was recovered from 1760 m water depth (Bale *et al*., 2019). The core was scanned at mm-scale using an Avaatech XRF Core Scanner (XCS) at the NIOZ (see Hennekam *et al*., 2019, 2020 for details) and Mo counts were converted to concentrations using ICP-MS analysis on discrete samples and a multivariate log-ratio approach for calibration (Weltje *et al*., 2015; Bale *et al*., 2019; Hennekam *et al*., 2020). Bulk rock digests were spiked with a ^{100}Mo-^{97}Mo double spike (Klaver and Coath, 2019) and Mo was separated from matrix and interferences using a scaled-down down (~10-fold, 200 µl resin-bed) version of a column chromatography procedure with AG1-X8 resin (Dickson *et al*., 2016). Mo-isotope data were measured in 2 % HNO_3 on a Thermo Scientific Neptune Plus MC-ICP-MS at the NIOZ and reported as $\delta^{98}Mo = [^{98/95}Mo_{sample}/^{98/95}Mo_{NIST}$ –

1] x 1000 + 0.25. The external reproducibility was estimated by analysis of the SDO-1 rock standard (1.00 ± 0.06 ‰, 2 s.d., n = 11). The age model of core 64PE406-E1 was constructed by alignment of sapropel boundaries for sapropels S1 to S' with well-dated nearby cores, *i.e.* LC21 (Grant *et al.*, 2016) for sapropels S1 to S5 and ODP 968 (Ziegler *et al.*, 2010) for Sapropels S6 to S'.

Results

δ^{98}Mo values range from -0.67 to +2.13 ‰ with an average of 0.91 ‰ (n = 64, Fig. S-1). The data table is available for download (Excel file) at https://www.geochemicalperspectivesletters.org/article2108. All samples are highly enriched in Mo relative to upper continental crust compositions, with Mo_{EF} (= $[Mo/Al]_{sample}/[Mo/Al]_{detrital}$) ranging from 21 to 201 with an average of 97, for an $Mo/Al_{detrital}$ ratio of 11.9 x 10^{-6} (Taylor and McLennan, 1985; Andersen *et al.*, 2018). Lowest δ^{98}Mo values (-0.4 to +0.2 ‰) are registered for sapropels S3 and S9. Together with S4 and S8, these sapropels also generally show the lowest Mo concentrations (<62 ppm for samples measured by ICP-MS). Highest δ^{98}Mo values (<2.13 ‰) and Mo concentrations (<140 ppm) are found for sapropels S5 and S7. Sapropel S6 shows intermediate Mo concentrations (<103 ppm) and δ^{98}Mo values (<1.53 ‰).

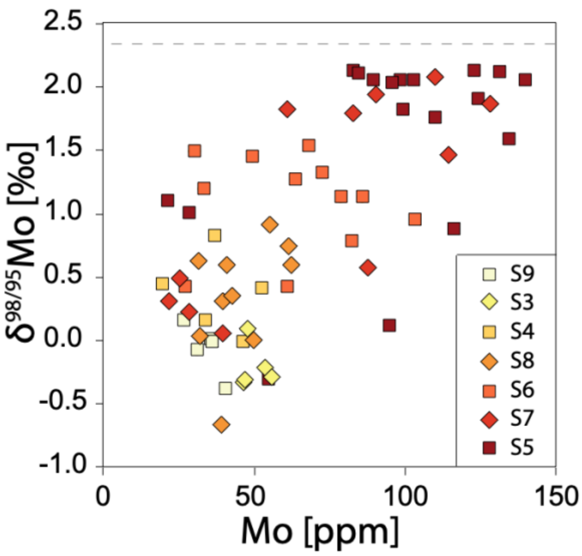

Figure S-1 δ^{98}Mo values relative to Mo concentrations for the different sapropels.

Comparison with other sapropel S5 data

Stratigraphic trends and absolute values of δ^{98}Mo and Mo concentrations of the sapropel S5 data presented in this study are generally very similar to previously published data (Fig. S-2; ODP 967 C, Andersen *et al*., 2018). The main difference between the two datasets is found near the onset of the sapropel interval, where data from the 64PE406-E1 core (this study) show considerably lower δ^{98}Mo values. This difference might be the result of the depth difference between the two locations. Larger isotopic fractionation between sediments and seawater might have been preserved for the 64PE406-E1 core location due to less reducing conditions at shallower depths. Alternatively, the lower sample resolution of the ODP 967 C core data might exclude the short perturbation to lower δ^{98}Mo values.

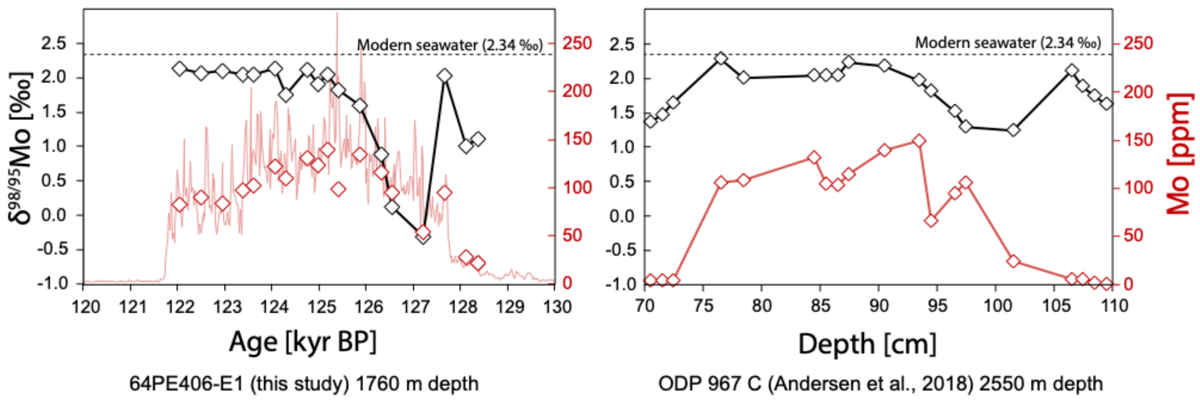

Figure S-2 Comparison of sapropel S5 Mo concentration and isotope data for the 64PE406-E1 core (this study) and ODP 967 C (Andersen *et al*., 2018).

Alternative models for low δ^{98}Mo values

The main manuscript focuses on the interpretation of Mo-isotope patterns as a result of varying H_2S concentrations. It suggests that low δ^{98}Mo values are the result of deposition in mildly euxinic conditions, as has also been proposed for sediments from the sapropel S1 interval (Azrieli-Tal *et al*., 2014; Matthews *et al*., 2017; Andersen *et al*., 2020). However, other models for low δ^{98}Mo values in sapropel or organic-rich sediments have also been suggested. The relevance of these alternative theories for low δ^{98}Mo values of the sapropel S3 to S9 data presented here will be discussed below.

Oxic (MnO_x) deposition and diagenetic alteration. Reitz *et al*. (2007) proposed that low δ^{98}Mo values for the partly oxidised sapropel S1 are the result of original oxic deposition of isotopically light Mo (MnO_x adsorption) and subsequent diagenetic alteration. This interpretation is largely based on an extremely high peak in Mn concentrations (up to ~25 %) for the oxidised top of the sapropel, which is associated with the highest Mo concentrations. The authors hypothesise that deposition of MnO_x was associated with adsorbed isotopically light Mo that was subsequently released to sedimentary pore waters during reductive dissolution of MnO_x. A fraction of the released Mo might have diffused upwards and precipitate with MnO_x at shallower sediment depths, whereas secondary uptake of Mo by authigenic sulphides might have led to additional Mo-isotope fractionation deeper in the sediment, possibly resulting in even lower δ^{98}Mo values. Later studies from other locations have generally suggested that low δ^{98}Mo values for the sapropel S1 interval are the result of large isotope fractionation from seawater under mildly euxinic conditions (Azrieli-Tal *et al*., 2014; Matthews *et al*., 2017; Andersen *et al*., 2020).

Mn concentration data for sapropels S3 to S9 do not provide direct support for the alternative model of MnO_x deposition as an explanation for low δ^{98}Mo values for these sapropels (Figs. S-3 and S-4). While depth intervals of enhanced Mn enrichments are observed for some sapropels, these peaks occur below the sapropel intervals and concentrations are much lower (<2 %) than Mn concentrations found near the top of the oxidised S1 interval (Fig. S-4). Samples with high Mn concentrations are not associated with high Mo concentrations or low δ^{98}Mo values (Fig. S-3). Additionally, low δ^{98}Mo values are found even for sapropels without increases in Mn concentrations around the sapropel interval (*e.g.*, S8 and S9). We therefore do not find direct support for original oxic deposition (MnO_x adsorption) as an explanation for low δ^{98}Mo values for the studied sapropels.

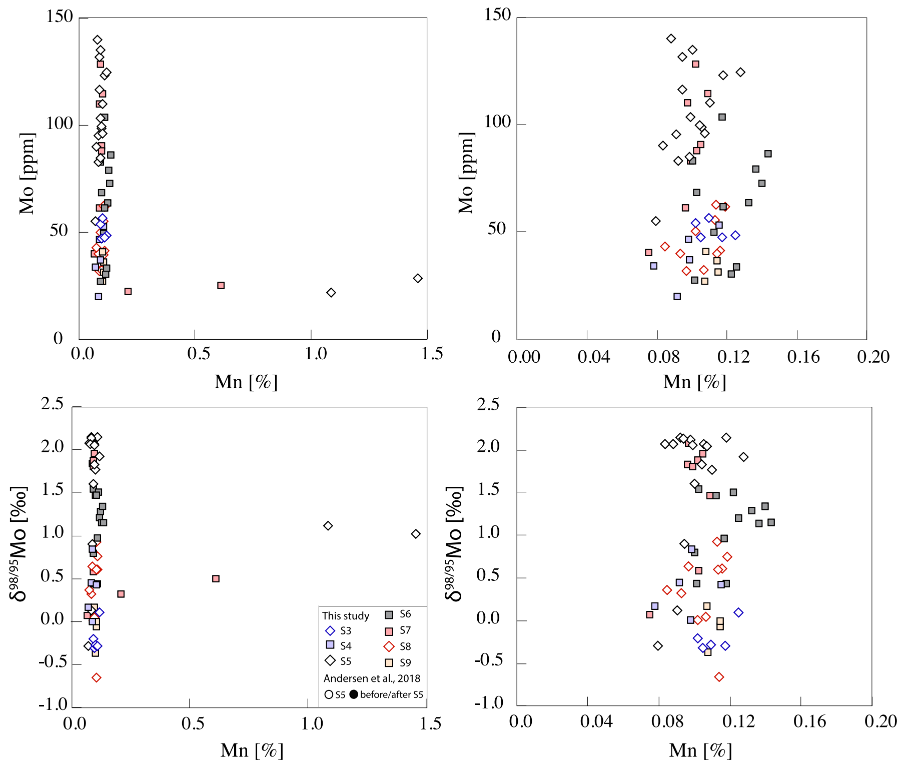

Figure S-3 δ^{98}Mo values and Mo concentrations relative to Mn concentrations. Apart from four outliers, Mn concentrations are generally low (<0.15 %). No correlations between Mn and Mo are observed.

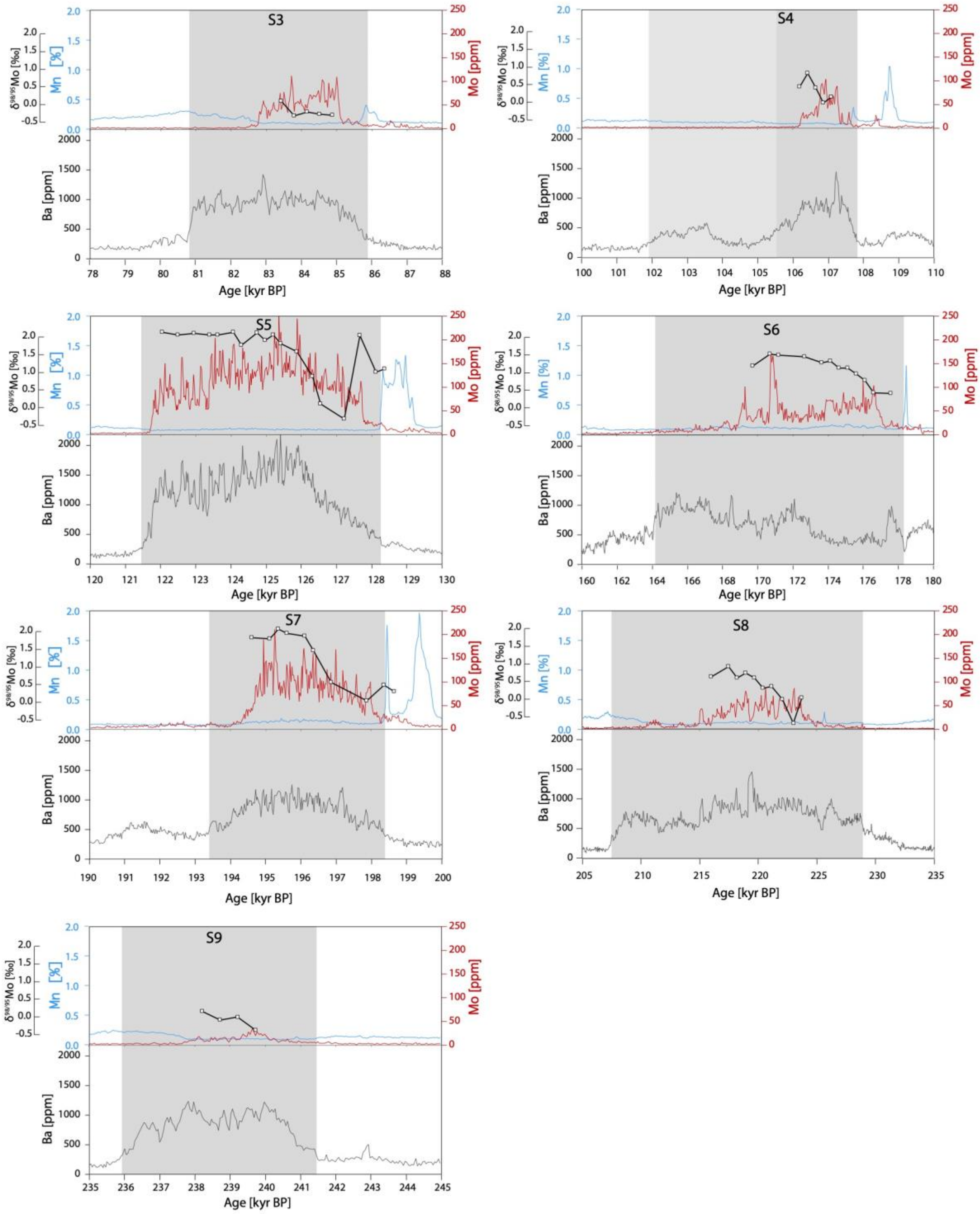

Figure S-4 Stratigraphic presentation Mo-isotope data with Ba, Mn, and Mo concentrations by XRF core scanning. The grey bands reflect the sapropel intervals as based on Ba enrichments.

Fe-Mn particulate shuttle. The delivery of isotopically light particulate Mo to the sediment with Fe (oxyhydr)oxides has also been suggested to cause light Mo-isotope signatures in some settings (*e.g.*, Scholz *et al*., 2017). A so-called Fe-Mn particulate shuttle may result in the enhanced transport of isotopically light Mo to the sediment followed by capture in authigenic Mo-S phases during early diagenesis (Algeo and Tribovillard, 2009). This process is considered to be particularly important in settings with oxic surface waters and nitrogenous deep waters, especially where short time-scale changes in redox conditions occur, as this allows the efficient shuttle of particulate Mo to the sediment because reactive Fe can repeatedly be recycled. Mo_{EF} *vs* U_{EF} cross-plots can provide insight in whether this particulate shuttle was a relevant mechanism for Mo enrichment during sapropel deposition as this process will not affect U enrichments (Algeo and Tribovillard, 2009). High Mo enrichments relative to U may therefore point to an active particulate Mo shuttle (Algeo and Tribovillard, 2009).

Mo_{EF} and U_{EF} patterns for the studied sapropels generally follow the unrestricted open marine trend and approach seawater values during peak-sapropel intervals, in agreement with previously published S1 and S5 data (Azrieli-Tal *et al*., 2014; Matthews *et al*., 2017; Andersen *et al*., 2018). These observations do not suggest that enhanced enrichment of Mo due to a strong Fe-Mn particulate shuttle was relevant during sapropel deposition. We therefore do not find direct support for an Fe-Mn particulate shuttle as an explanation for the low δ^{98}Mo values for these sapropels and conclude that these likely derive from a large isotopic fractionation in mildly euxinic conditions, as also suggested in recent studies of sapropel S1 (Azrieli-Tall *et al*., 2014; Matthews *et al*., 2017; Andersen *et al*., 2020).

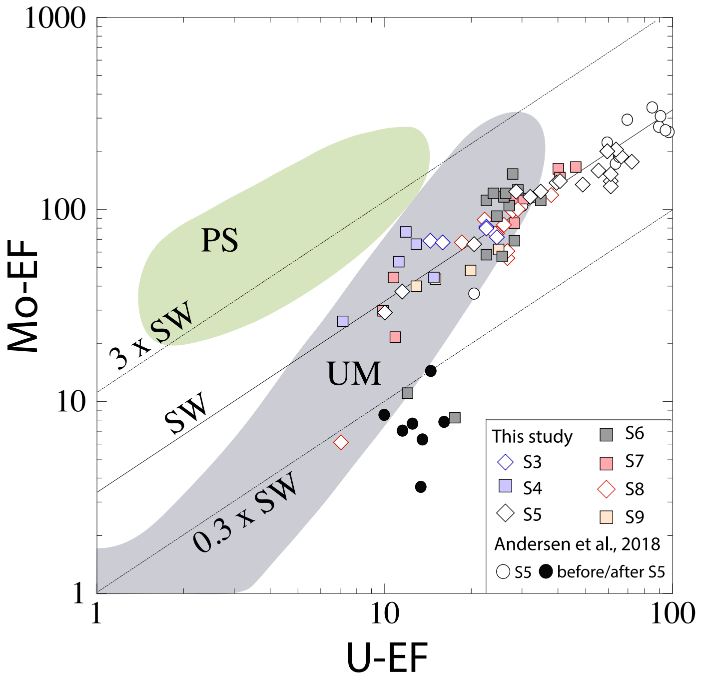

Figure S-5 Mo_{EF} *versus* U_{EF} cross-plots after Algeo and Tribovillard (2009). The green area reflects enhanced Mo enrichment linked to operation of an Fe-Mn particulate shuttle, whereas the grey area reflects values found in unrestricted marine conditions. Samples from sapropel intervals generally plot close to the open ocean seawater ratio. Previously published S5 data is added for comparison (Andersen *et al*., 2018).

Supplementary Information References

Algeo, T.J., Tribovillard, N. (2009) Environmental analysis of paleoceanographic systems based on molybdenum–uranium covariation. *Chemical Geology* 268, 211-225.

Andersen, M.B., Matthews, A., Vance, D., Bar-Matthews, M., Archer, C., de Souza, G. (2018) A 10-fold decline in the deep Eastern Mediterranean thermohaline overturning circulation during the last interglacial period. *Earth and Planetary Science Letters* 503, 58-67.

Andersen, M.B., Matthews, A., Bar-Matthews, M. Vance, D. (2020) Rapid onset of ocean anoxia shown by high U and low Mo isotope compositions of sapropel S1. *Geochemical Perspectives Letters* 15, 10-14.

Azrieli-Tal, I., Matthews, A., Bar-Matthews, M., Almogi-Labin, A., Vance, D., Archer, C., Teutsch, N. (2014) Evidence from molybdenum and iron isotopes and molybdenum–uranium covariation for sulphidic bottom waters during Eastern Mediterranean sapropel S1 formation. *Earth and Planetary Science Letters* 393, 231-242.

Bale, N.J., Hennekam, R., Hopmans, E.C., Dorhout, D., Reichart, G.-J., van der Meer, M., Villareal, T.A., Sinninghe Damsté, J.S., Schouten, S. (2019) Biomarker evidence for nitrogen-fixing cyanobacterial blooms in a brackish surface layer in the Nile River plume during sapropel deposition. *Geology* 47, 1088-1092.

Dickson, A.J., Jenkyns, H.C., Porcelli, D., van den Boorn, S., Idiz, E. (2016) Basin-scale controls on the molybdenum-isotope composition of seawater during Oceanic Anoxic Event 2 (Late Cretaceous). *Geochimica et Cosmochimica Acta* 178, 291-306.

Grant, K., Grimm, R., Mikolajewicz, U., Marino, G., Ziegler, M., Rohling, E. (2016) The timing of Mediterranean sapropel deposition relative to insolation, sea-level and African monsoon changes. *Quaternary Science Reviews* 140, 125-141.

Hennekam, R., Sweere, T., Tjallingii, R., de Lange, G.J., Reichart, G.-J. (2019) Trace metal analysis of sediment cores using a novel X-ray fluorescence core scanning method. *Quaternary International* 514, 55-67.

Hennekam, R., van der Bolt, B., van Nes, E.H., de Lange, G.J., Scheffer, M., Reichart, G.-J. (2020) Early-warning signals for marine anoxic events. *Geophysical Research Letters* 47, e2020GL089183.

Klaver, M., Coath, C.D. (2019) Obtaining Accurate Isotopic Compositions with the Double Spike Technique: Practical Considerations. *Geostandards and Geoanalytical Research* 43, 5-22.

Matthews, A., Azrieli-Tal, I., Benkovitz, A., Bar-Matthews, M., Vance, D., Poulton, S.W., Teutsch, N., Almogi-Labin, A., Archer, C. (2017) Anoxic development of sapropel S1 in the Nile Fan inferred from redox sensitive proxies, Fe speciation, Fe and Mo isotopes. *Chemical Geology* 475, 24-39.

Reitz, A., Wille, M., Nägler, T.F., de Lange, G.J. (2007) Atypical Mo isotope signatures in eastern Mediterranean sediments. *Chemical Geology* 245, 1-8.

Rudnick, R.L., Gao, S. (2003) Composition of the continental crust. In: Holland, H., Turekian, K. (Eds.) *Treatise on Geochemistry*, Second Edition. Elsevier, 1-64.

Scholz, F., Siebert, C., Dale, A.W., Frank, M. (2017) Intense molybdenum accumulation in sediments underneath a nitrogenous water column and implications for the reconstruction of paleo-redox conditions based on molybdenum isotopes. *Geochimica et Cosmochimica Acta* 213, 400-417.

Taylor R.N., McLennan, S. (1985) *The Continental Crust: Its Composition and Evolution*. Blackwell, Boston.

Weltje, G.J., Bloemsma, M., Tjallingii, R., Heslop, D., Röhl, U., Croudace, I.W. (2015) Prediction of geochemical composition from XRF core scanner data: a new multivariate approach including automatic selection of calibration samples and quantification of uncertainties. In: Croudace, I.W., Rothwell, R.G. (Eds.) *Micro-XRF Studies of Sediment Cores*. Springer, Dordrecht, 507-534.

Ziegler, M., Tuenter, E., Lourens, L.J. (2010) The precession phase of the boreal summer monsoon as viewed from the eastern Mediterranean (ODP Site 968). *Quaternary Science Reviews* 29, 1481-1490.